INTERNATIONAL JOURNAL OF MULTIDISCIPLINARY RESEARCH AND ANALYSIS

ISSN(print): 2643-9840, ISSN(online): 2643-9875

Volume 07 Issue 07 July 2024

DOI: 10.47191/ijmra/v7-i07-05, Impact Factor: 8.22

Page No. 3101-3109

Prepare Aromatic Derivatives of Nanosheets by a Specially Designed Electrolytic Cell

Ghazwan H. Abd AL-Wahab[1], Tariq B. Mahmood[2], Ammar S. Mohammed[3]

[1]Tikrit University

[2]Salah al-Din Education Directorate

[3]Kirkuk University

ABSTRACT: This research includes the preparation of aromatic derivatives of nanosheets by the electrochemical method ArCBG **,I)**II) by a specially designed electrolytic cell (SDEC) in two steps: The first step: prepare diazonium salts by using one of the amines(4-Aminobenzoic Aminophenazonand second- (e 4 ,acidstep: Preparation of highly aromatic nanosheets carbon-by used CBG nano was dissolved in800 ml of distilled water and then .placed in an ultrasonic bath The compounds were diagnosed using FT-IR, XRD, FE.SEM and AFM

KEYWORDS: Nano, Electrolytic Cell, Electrochemical, Graphene.

1. INTRODUCTION:

Nanomaterials include wide groups of materials, which have been classified according to their chemical nature, where they can be formed in the form of a compound as in nano zinc oxide or be in the form of a single element as in nano gold, such as copper and zinc oxide on graphene oxide [1, 2]. Nanomaterials have been classified into natural and industrial materials (smoke from fuel combustion and volcanic ash) [3]. There is another classification of nanomaterials, which depends on the dimensions of nanoparticles, which are subject to the nanoscale and therefore can be classified into four main sections, namely, materials Zero-dimensional nanomaterials, one-dimensional nanomaterials, two-dimensional nanomaterials, and three-dimensional nanomaterials [4, 5]. The nanomaterials were divided into two main parts. The first section starts from the top to the bottom, where the original (large) material is broken until the nano size is reached [6]. There are several methods used to achieve this, the most famous of which are (fragmentation, grinding, cutting, and optical engraving), where these techniques were used to obtain microscopic electronic compounds such as computer chips [7, 8], and the second section starts from the bottom up, unlike the first method [9]. The nanomaterial is built starting from atoms and molecules arranged until it reaches the desired secondary shape and size [10]. This method is included in the mold within the chemical methods [11]. It is characterized by the small size of the resulting materials and the lack of losses, and in addition to obtaining bonds, Strong nanomaterial is produced. Let's look at the first section (from top to bottom) [12]. We will find that some techniques that appeared more than 20 years ago could prepare beads of material with very small dimensions, among these techniques (quick cooling techniques or Solution-gel techniques) [13, 14]. Graphite is one of the many forms of carbon, as each carbon atom is triple bonded with three other carbon atoms located within the same space plane, until we finally get hexagonal fused rings, like the geometric shape in aromatic hydrocarbons [15], Since graphite is multilayered and has a plane structure and its atoms are covalently attached to three valence electrons, while the fourth electron remains free, and this explains the high conductivity of graphite, as they are linked to each other by means of (Vander Walls Forces) and this makes it easy the separation between its layers, as graphite has received great attention by nanotechnology scientists, due to its two important properties: (Strength and electrical conductivity [16 ,17], and graphene oxide is produced graphite oxide by treating the graphite with a solution of sulfuric acid, sodium nitrate and potassium permanganate according to the modified Hammer method [18], then the graphene oxide is reduced using strong reducing agents to obtain reduced graphene oxide [19]. It is one of the available materials and has multiple uses, including in the chemical industries, such as the production of phosphorous and calcium [21, 22].

2. EXPERIMENTAL

2.1. Chemicals used: All chemicals used in this work were purchased from BDH, Aldrich and Fluka companies and were used without further purification.

2.2. Devices used: The melting points were measured using Electrothermal Melting Apparatus 9300. The FT-IR spectra were captured using a Shimadzu FT-IR 8400S spectrophotometer with a (400-4000) cm-1 by KBr disc. Scanning Electron Microscopy (SEM) A scanning electron microscope was used to obtain information about the surface and the dimensions in which the particles are compacted with the dimensions of the particles themselves. X-ray diffraction machine using a device (Shimadzu-XRD-6000) with a nickel-copper filter for X-ray radiation (CuKa, A=1.5406A), the target is the X-ray-producing copper material at 30 kv and current mA 30, The survey was conducted over a range of 2Θ (80,000-2,000), continuously and at a rate of speed (2°/min), 0.3mm diameter entry aperture, Kashan University, Iran. Atomic Force Microscopy (AFM) the device was used (AFM icon. Bruke Q600 (US) at Kashan University - Iran.

2.3. Prepare aromatic derivatives of nanosheets by the electrochemical method ArCBG (I, II) by a specially designed electrolytic cell [23, 23]:

First step: prepare diazonium salts

The preparation was prepared by dissolving 6.4 g of one of the amines (4-Aminobenzoic acid, 4-Aminophenazone) in a beaker containing acid solution (160:160 water: concentrated hydrochloric acid 37%) while maintaining the temperature of the solution Within (0-5) 0 C with continuous stirring, and in another beaker, dissolve 2.24 g of sodium nitrite in the least possible amount of distilled water and add to the first solution while keeping the temperature within the range (0-5) 0 C using an ice bath with stirring Continuous for 30 minutes in dark weather (6), not diagnosed but used directly in step 2.

Second step: Preparation of highly aromatic nanosheets

3.2 g of the prepared CBG nano-carbon was dissolved in 800 ml of distilled water and then placed in an ultrasonic bath until the solution became clear. The solution was added to the electrolytic cell (SDEC: consisting of two voltage-connected platinum electrodes). 1.6 V with continuous stirring, then the solution of the first step was added to it with cooling in an ice bath, and the cell remained on continuous stirring for 24 hours continuously. The solution was washed with ionic water several times and filtered with nano vacuum (7), As in Figure 2-3, and left to dry until the weight was stable.

3. RESULTS AND DISCUSSION:

Nano-derivatives and compounds were prepared, the first source of which is the charred parts of the straw, where the nano-reduced graphene oxide and graphite are partial, through the steps shown in the following diagrams:

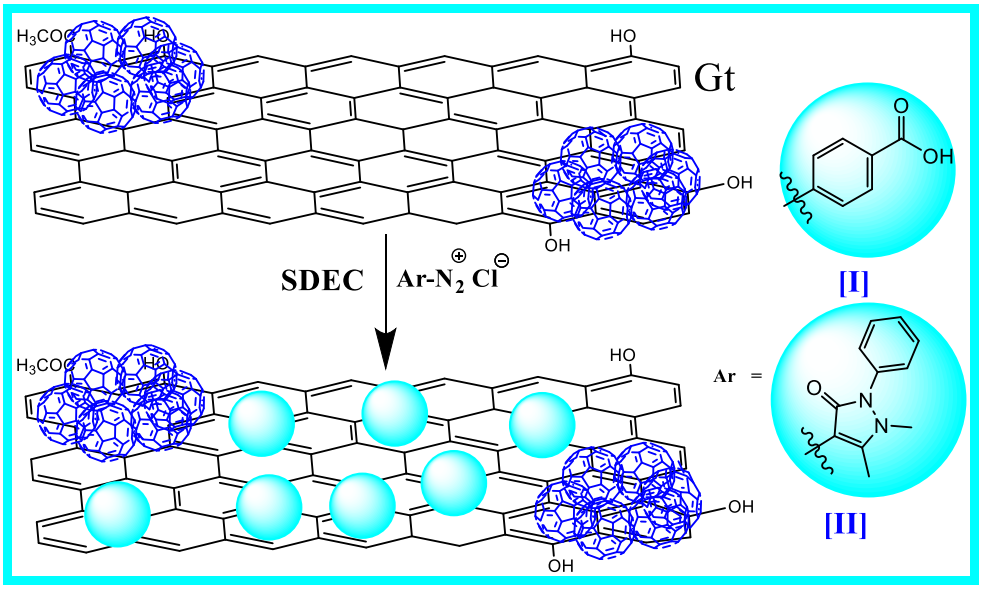

Scheme (1): Preparation of compounds (I, II)

Compound (I) was prepared from the reaction of the diazonium salt of 4-aminobenzoic acid (4-Aminobenzoic acid) with WSGt carbon nanosheets, then the electrical reaction was completed using the electrolytic cell.

The reaction begins with the formation of the diazonium salt in the first step, then a molecule (N≡N) is released and the formation of the carbonium ion in the second step, which in turn binds with the nano-carbon to form the nanocomposite (I, II) [25], and according to the mechanical the following is suggested:

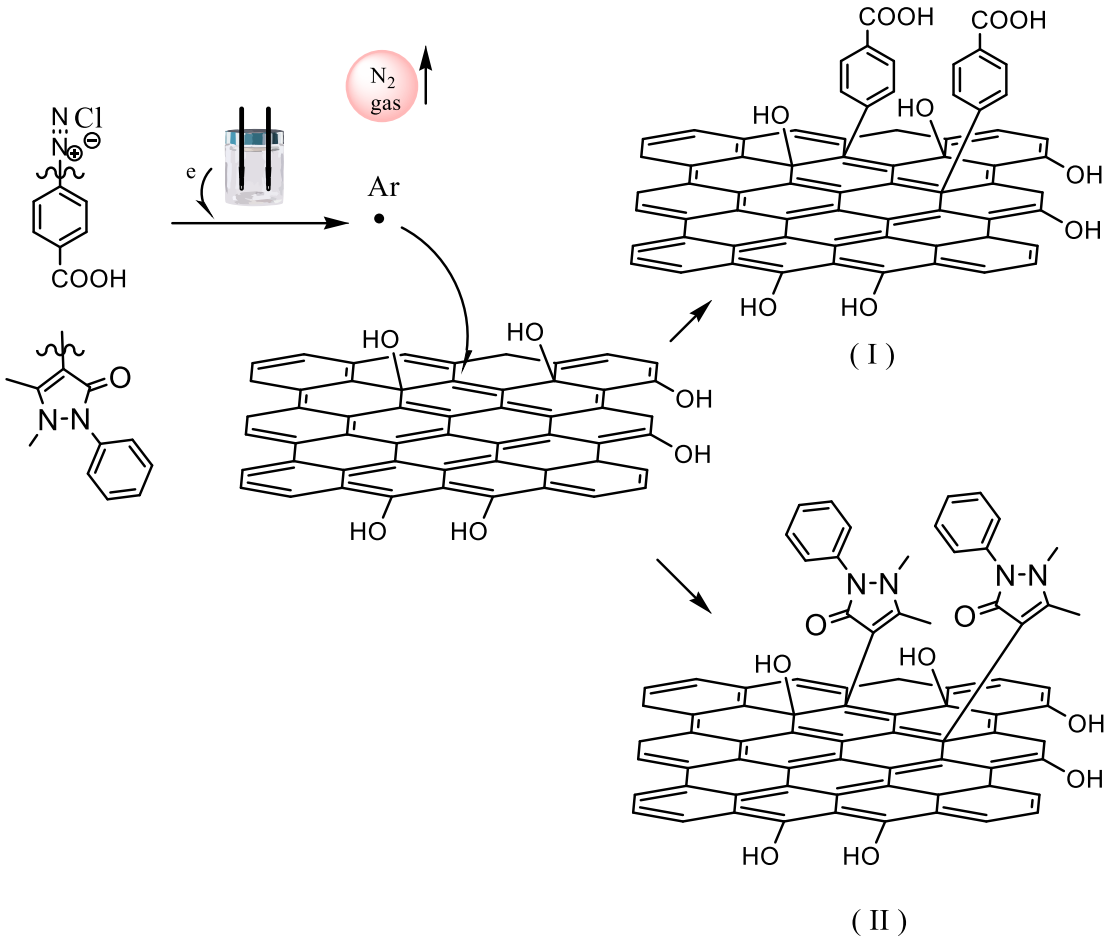

Scheme (2): Preparation mechanism of compounds (I, II)

3.1. Characterization of (I):

Where when studying the infrared (IR) spectrum of the prepared compound [I], it was found that a beam appeared at a frequency (3390) cm-1 belonging to the (OH) group, and a beam appeared at a frequency (3070) cm- 1 belongs to the aromatic (CH) group, and two bands appear at frequency (2947, 2879) cm-1 belonging to the aliphatic (CH) group, and an absorption band appears at frequency (1718) cm-1 belonging to the carbonyl group (C=O) carboxylic, and the appearance of two absorption bands at the frequency (1598, 1487) cm-1 due to the stretching of the aromatic (C=C) bond, and the appearance of an absorption band at the frequency (1340) cm-1 due to the group (C=O) C-O), and as shown in figure (1), these packages for diagnosing the two samples were close to what is found in the literature [26, 27].

While the X-ray spectrum of the compound [I] showed an angle value of 2θ at 27.5270 with interlayer distances d=3.24040 with a grain size of D=52.05 and several layers n=16.06283, It was noted that these values are close to the literature [28, 29], it is noted in figure (2).

From the morphological FESEM images of the sample I shown in figure (3), crusting was observed in sample a with more transparent thickenings in sample b, both within the nanoscale and on the edges and surface of the plate, higher transparency for plates c and the appearance of less elasticity for plates d, and this indicates a better preparation efficiency in the cell and this is due to the quality of the peeling and the need for a higher voltage difference to reach better peeling and greater flexibility of the plates [30, 31].

The topography of the surface was studied using AFM for the compound I. The images showed the presence of peaks scattered on the plates at different heights while it was less sharp and wavier with peaks height of up to 50 in b in c, which showed A horizontal pattern with volcanic heights of the peaks. The images also showed a greater differentiation of the plates in d [32, 33], which is noted in figure (4).

3.2. Characterization of (II):

When studying the infrared (I.R.) spectrum of the prepared compound [II], it was noticed that a beam appeared at a frequency (3336) cm-1 belonging to the (O.H.) group. A beam that appeared at the frequency (3035) cm-1 belonging to the aromatic (C.H.) group. Two bands at a frequency (2970, 2858) cm-1 belong to the aliphatic (C.H.) group, a band appears at (1693) cm-1 belongs to

the (C.H.) group C = O), and the appearance of two absorption bands at the frequency (1587, 1488) cm-1 due to the stretching of the aromatic (C = C) band, and the appearance of the absorption band at the frequency (1135) cm-1 due to the stretching of the (C-N) bond). The appearance of an absorption band at a frequency of (1020) cm-1 belonging to the (N-N) group, and as shown in figure (5), and these bands for diagnosing the two samples were identical to each other and to what is found in the literature [34, 35].

The X-ray spectrum of the compound [II] showed an angle value of 2θ at 22.9501 with interlayer distances d=3.87520, a grain size of D=8.21, and several layers n=2.11860. It was noted that these values are close to the literature [36, 37]. It is noted in figures (6). From the FESEM morphological images of the sample II shown in figure (7), it was observed that there were distinct geometric sheets a that was thicker, with a clearness of the slab's capacity and the spread of decoration on it more uniformly b with the appearance of Geometric shapes focused on decoration and three-armed star holes, while c showed clusters on the edges with more obvious cracks, clusters with larger nanoscale values in d, and this indicates the ability of D.E. to provide a good surface for spreading and reduce plate deformation—formed where it maintains a pattern of cracks similar to what was mentioned in the literature (one of my books) around graphene surfaces [38, 39].

The topography of the surface was studied using AFM of the compound II. Images a showed a clearer spread of decoration in II, lower heights of peaks in II, and conical shapes of peaks appear in sample c, with appearance of a larger capacity of the plates in d, see figure (8).

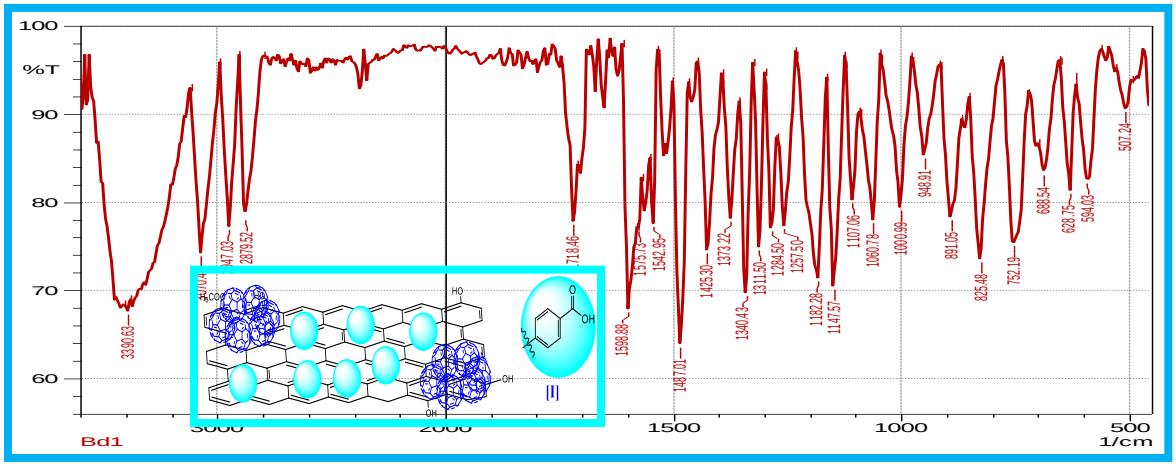

Figure (1): Infrared spectrum of the nanocomposite (I)

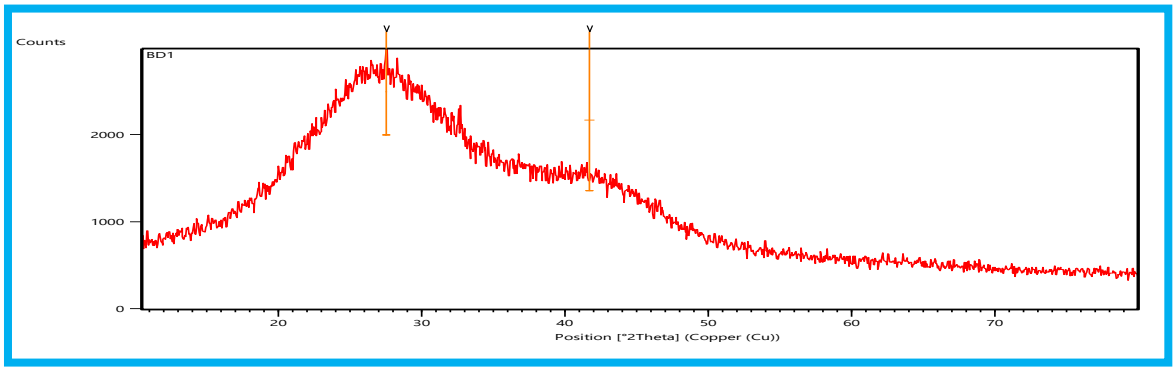

Figure (2): X-ray spectrum of the compound (I)

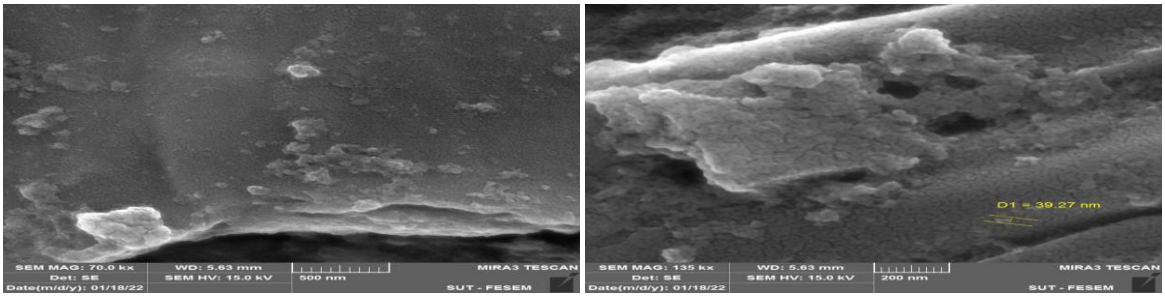

A B

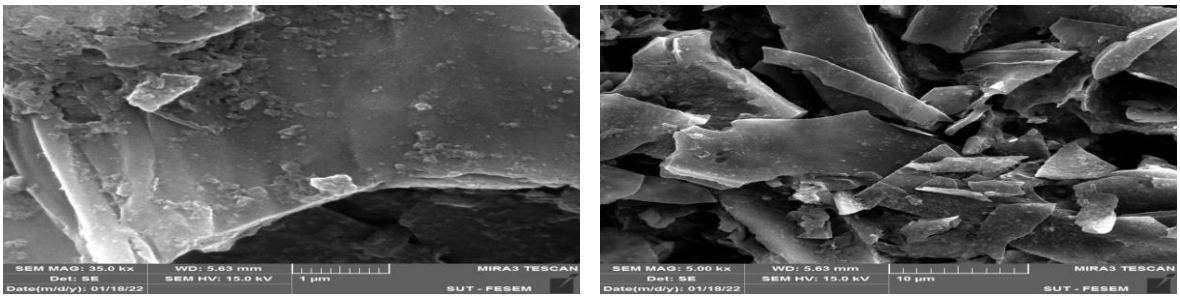

C D

Figure (3): FESEM images of the compound (I)

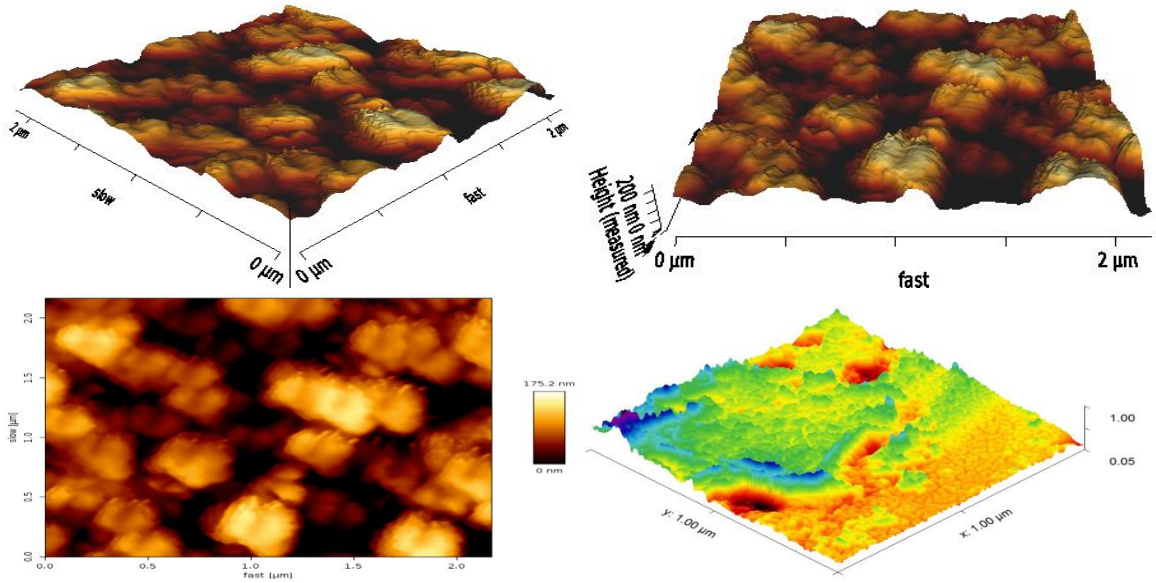

Figure (4): AFM images of the compound (I)

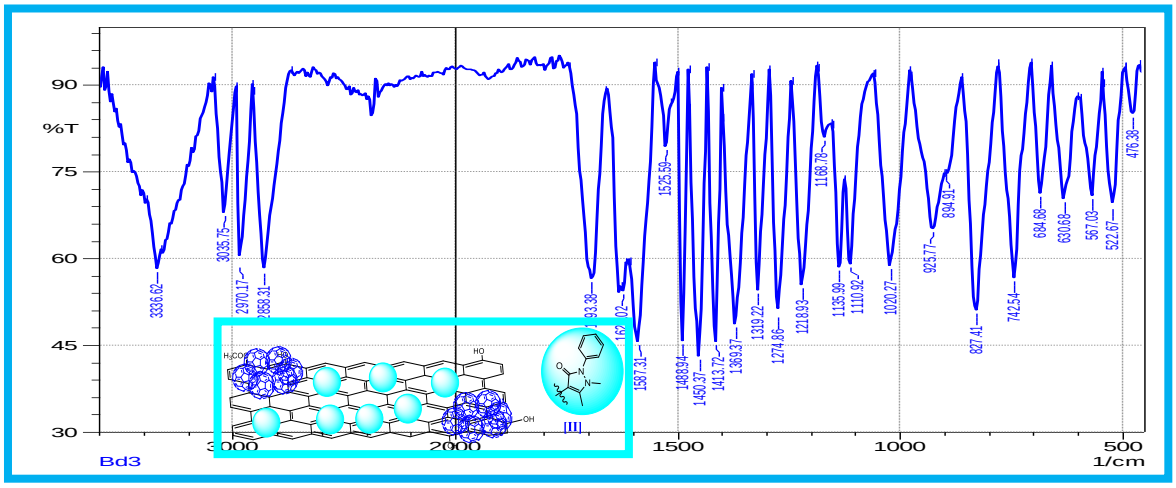

Figure (5): Infrared spectrum of the nanocomposite (II)

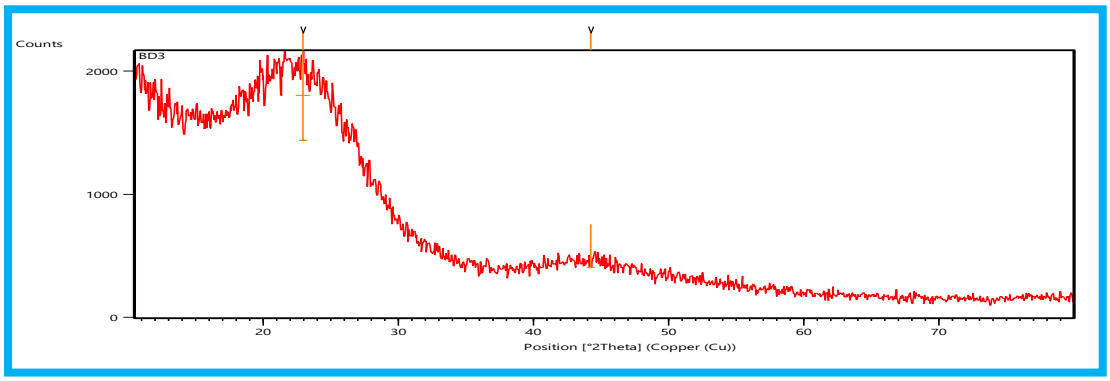

Figure (6): X-ray spectrum of the compound (II)

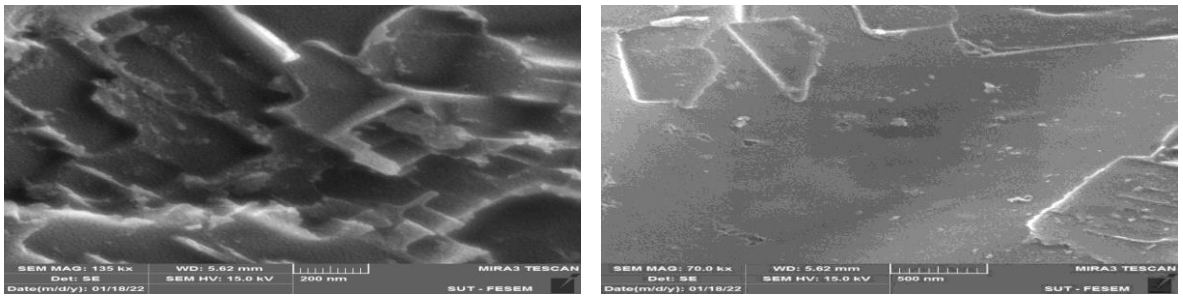

a B

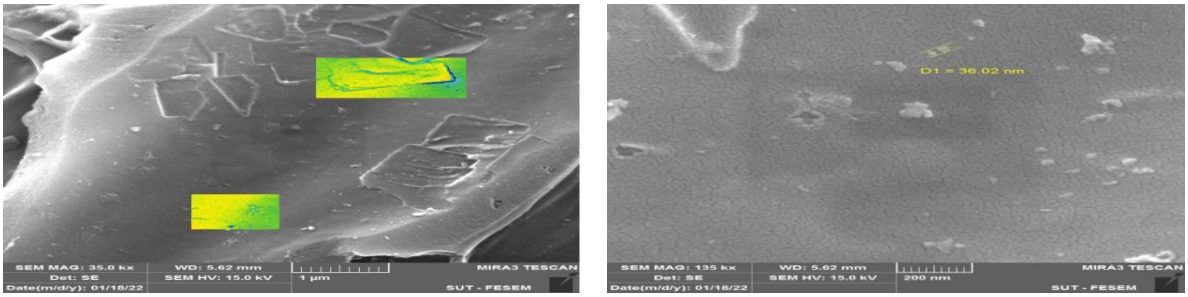

c d

Figure (7): FESEM images of the compound (II)

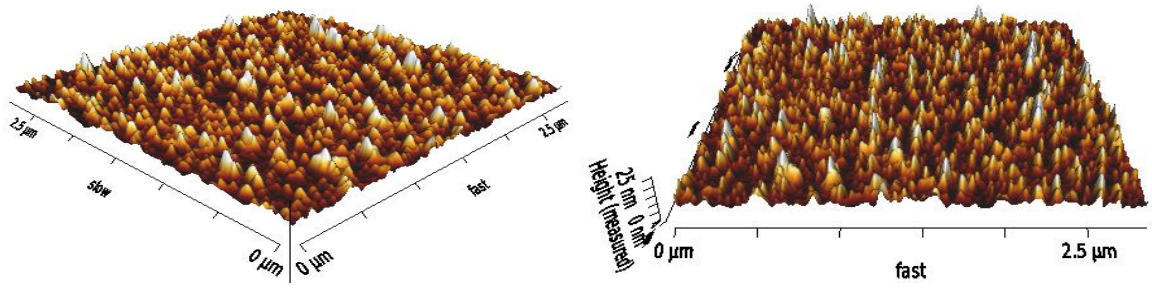

a b

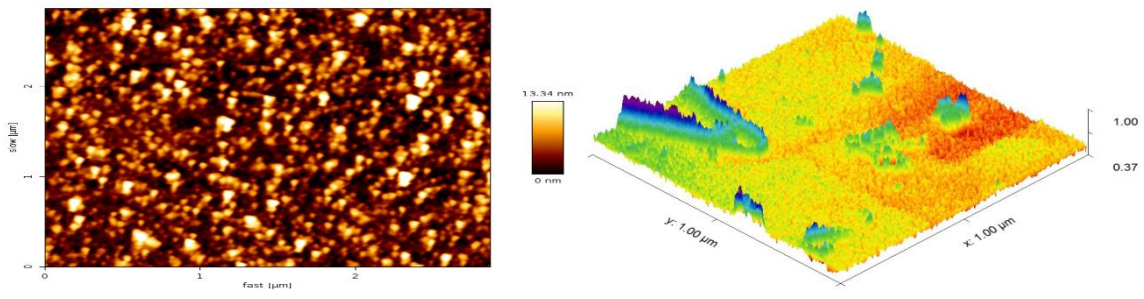

c d

Figure (8): AFM images of the composite (II)

4. CONCLUSIONS

Physical and spectroscopic measurements validated the produced compounds' correctness and validity. As a result, the preparation procedures were effective, efficient, and low-cost. The microanalysis results of the compounds' components were exactly or almost equivalent to the estimated proportion. The increase in the number of layers indicates the reduction and the convergence of layers in a single crystal. The relationship is not always direct between the peaks of the grain size D and the number of layers n or the distances between them d, which is due to the difference in the compositions of additives. The relationship between the surface roughness and the average height is a direct relationship. A large number of crust gaps indicates the highest value of the roughness deviation; from this, we infer that the relationship is direct. The fact that the hydrogen bonds increase the stratification and grain size explains the anomaly in the grain size values of some of the prepared nanocomposites.

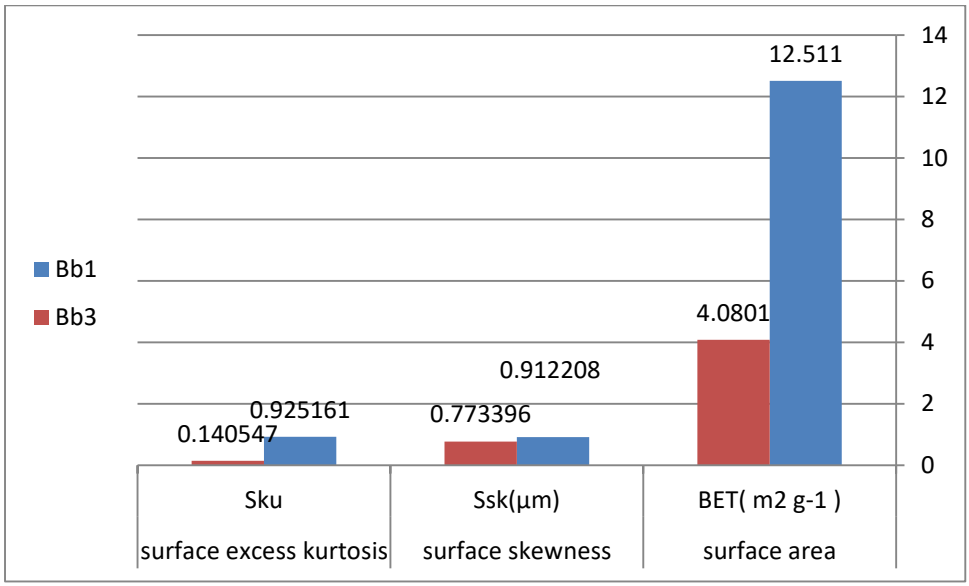

Figure (9) of the curve of the relationship between so-and-so and so-and-so for the prepared samples (I , II)

From the curve, it was observed that the porosity of the two samples differed, as well as a direct relationship between the BET surface area of the samples and both the roughness deviation Ssk and the curvature Sku, and this can be explained as follows

The relationship between the structure and the surface area of BET can be explained by the increase in the releasing ability of diazonium salt to nitrogen gas between the plates during the process of electron capture from the cell This is due to the fact that the carboxylic group in the para-site of I increases the electrophilic character of the para-carbon carrying the diazo group, making it more capable of receiving an electronThus, it is more capable of releasing nitrogen gas between the layers, which leads to an increase in peeling and an increase in the surface area, , compared with the unsaturated cyclic alpha, beta system in the compound II, which provides a permanent electronic density in the alpha site with respect to the carbonyl group, thus the electrophilicity of the diazo grouping carbon decreases and the release of nitrogen gas during the reaction decreases, and thus an expected decrease in the surface area.

As for the fact that Ssk < 0 (peaks dominate) and Sku < 3 (equatorial ones dominate very little), these two factors indicate that the ratio of flat surfaces is predominant in the stratified groups, while the peaks are predominant in cases of high exfoliation.

REFERENCES

1) Sun, X., Liu, Z., Welsher, K., Robinson, J. T., Goodwin, A., Zaric, S., & Dai, H. (2008). Nano-graphene oxide for cellular imaging and drug delivery. Nano research, 1(3), 203-212.
2) Gonçalves, G., Vila, M., Portolés, M. T., Vallet-Regi, M., Gracio, J., & Marques, P. A. A. (2013). Nano-graphene oxide: a potential multifunctional platform for cancer therapy. Advanced healthcare materials, 2(8), 1072-1090.
3) Seabra, A. B., Paula, A. J., de Lima, R., Alves, O. L., & Durán, N. (2014). Nanotoxicity of graphene and graphene oxide. Chemical research in toxicology, 27(2), 1
4) Tian, B., Wang, C., Zhang, S., Feng, L., & Liu, Z. (2011). Photothermally enhanced photodynamic therapy delivered by nano-graphene oxide. ACS nano, 5(9), 7000-7009.
5) Chuah, S., Pan, Z., Sanjayan, J. G., Wang, C. M., & Duan, W. H. (2014). Nano reinforced cement and concrete composites and new perspective from graphene oxide. Construction and Building materials, 73, 113-124.

6) Luo, J., Cote, L. J., Tung, V. C., Tan, A. T., Goins, P. E., Wu, J., & Huang, J. (2010). Graphene oxide nanocolloids. Journal of the American Chemical Society, 132(50), 17667-17669.
7) Wang, Y., Li, Z., Wang, J., Li, J., & Lin, Y. (2011). Graphene and graphene oxide: biofunctionalization and applications in biotechnology. Trends in biotechnology, 29(5), 205-212.
8) Cheng, M., Yang, R., Zhang, L., Shi, Z., Yang, W., Wang, D., ... & Zhang, G. (2012). Restoration of graphene from graphene oxide by defect repair. Carbon, 50(7), 2581-2587.
9) Yang, K., Gong, H., Shi, X., Wan, J., Zhang, Y., & Liu, Z. (2013). In vivo biodistribution and toxicology of functionalized nano-graphene oxide in mice after oral and intraperitoneal administration. Biomaterials, 34(11), 2787-2795.
10) Pei, X., Zhu, Z., Gan, Z., Chen, J., Zhang, X., Cheng, X., ... & Wang, J. (2020). PEGylated nano-graphene oxide as a nanocarrier for delivering mixed anticancer drugs to improve anticancer activity. Scientific reports, 10(1), 1-15.
11) Rahmanian, N., Hamishehkar, H., Dolatabadi, J. E. N., & Arsalani, N. (2014). Nano graphene oxide: a novel carrier for oral delivery of flavonoids. Colloids and Surfaces B: Biointerfaces, 123, 331-338.
12) Perrozzi, F., Prezioso, S., & Ottaviano, L. (2014). Graphene oxide: from fundamentals to applications. Journal of Physics: Condensed Matter, 27(1), 013002.
13) Ray, S. C. (2015). Application and uses of graphene oxide and reduced graphene oxide. Applications of graphene and graphene-oxide based nanomaterials, 1.
14) Jang, S. C., Kang, S. M., Lee, J. Y., Oh, S. Y., Vilian, A. E., Lee, I., & Huh, Y. S. (2018). Nano-graphene oxide composite for in vivo imaging. International journal of nanomedicine, 13, 221.
15) Dong, H., Zhao, Z., Wen, H., Li, Y., Guo, F., Shen, A., ... & Shi, D. (2010). Poly (ethylene glycol) conjugated nano-graphene oxide for photodynamic therapy. Science China Chemistry, 53(11), 2265-2271.
16) Ryoo, S. R., Lee, J., Yeo, J., Na, H. K., Kim, Y. K., Jang, H., ... & Min, D. H. (2013). Quantitative and multiplexed microRNA sensing in living cells based on peptide nucleic acid and nano graphene oxide (PANGO). ACS nano, 7(7), 5882-5891.
17) Delekta, S. S., Adolfsson, K. H., Erdal, N. B., Hakkarainen, M., Östling, M., & Li, J. (2019). Fully inkjet printed ultrathin microsupercapacitors based on graphene electrodes and a nano-graphene oxide electrolyte. Nanoscale, 11(21), 10172-10177.
18) Hu, X., Yu, Y., Wang, Y., Zhou, J., & Song, L. (2015). Separating nano graphene oxide from the residual strong-acid filtrate of the modified Hummers method with alkaline solution. Applied Surface Science, 329, 83-86.
19) Wen, H., Dong, C., Dong, H., Shen, A., Xia, W., Cai, X., ... & Shi, D. (2012). Engineered redox-responsive PEG detachment mechanism in PEGylated nano-graphene oxide for intracellular drug delivery. Small, 8(5), 760-769.
20) Chung, C., Kim, Y. K., Shin, D., Ryoo, S. R., Hong, B. H., & Min, D. H. (2013). Biomedical applications of graphene and graphene oxide. Accounts of chemical research, 46(10), 2211-2224.
21) Yang, D., Feng, L., Dougherty, C. A., Luker, K. E., Chen, D., Cauble, M. A., & Hong, H. (2016). In vivo targeting of metastatic breast cancer via tumor vasculature-specific nano-graphene oxide. Biomaterials, 104, 361-371.
22) Adeel, M., Bilal, M., Rasheed, T., Sharma, A., & Iqbal, H. M. (2018). Graphene and graphene oxide: Functionalization and nano-bio-catalytic system for enzyme immobilization and biotechnological perspective. International journal of biological macromolecules, 120, 1430-1440.
23) Jabar, S. A., Hussein, A. L., Dalaf, A. H., & Aboud, H. S. (2020). Synthesis and Characterization of Azetidine and Oxazepine Compounds Using Ethyl-4-((4-Bromo Benzylidene) Amino) Benzoate as Precursor and Evalution of Their Biological Activity. Journal of Education and Scientific Studies, 5(16).
24) Dalaf, A. H. (2018). Synthesis and Characterization of Some Quartet and Quinary Hetero cyclic Rings Compounds by Traditional Method and Microwave Routes Method and Evaluation of Their Biological Activity. M.Sc. Thesis, Tikrit University, Tikrit, Iraq: 1-94 pp.
25) Dalaf, A. H., & Jumaa, F. H. (2018). Synthesis, Characterization of some 1,3-Oxazepane -4,7-Dione by Traditional and Microwave routes method and evaluation of their biological activity. Al-utroha for Pure Science. (8): 93-108.
26) Dalaf, A. H., Jumaa, F. H., & Jabbar, S. A. S. (2018). Synthesis and Characterization of some 2, 3-dihydroquinozoline and evaluation of their biological activity. Tikrit Journal of Pure Science, 23(8): 66-67.
27) Salwa, A. J., Ali, L. H., Adil, H. D., Hossam, S. A. (2020). Synthesis and Characterization of Azetidine and Oxazepine Compounds Using Ethyl-4-((4-Bromo Benzylidene) Amino) Benzoate as Precursor and Evalution of Their Biological Activity. Journal of Education and Scientific Studies, ISSN: 24134732. 16(5): 39-52.
28) Dalaf, A. H., & Jumaa, F. H. (2020). Synthesis, Identification and Assess the Biological and Laser Efficacy of New Compounds of Azetidine Derived from Benzidine. Muthanna Journal of Pure Science (MJPS), 7(2):12-25.

29) Saleh, R. H., Rashid, W. M., Dalaf, A. H., Al-Badrany, K. A., & Mohammed, O. A. (2020). Synthesis of Some New Thiazolidinone Compounds Derived from Schiff Bases Compounds and Evaluation of Their Laser and Biological Efficacy. Ann Trop & Public Health, 23(7): 1012-1031.
30) Yass, I. A., Aftan, M. M., Dalaf, A. H., & Jumaa, F. H. (Nov. 2020). Synthesis and Identification of New Derivatives of Bis-1,3-Oxazepene and 1,3-Diazepine and Assess the Biological and Laser Efficacy for Them. The Second International & The Fourth Scientific Conference of College of Science – Tikrit University. (P4): 77-87.
31) Salih, B. D., Dalaf, A. H., Alheety, M. A., Rashed, W. M., & Abdullah, I. Q. (2021). Biological activity and laser efficacy of new Co (II), Ni (II), Cu (II), Mn (II) and Zn (II) complexes with phthalic anhydride. Materials Today: Proceedings, 43, 869-874.
32) Aftan, M. M., Jabbar, M. Q., Dalaf, A. H., & Salih, H. K. (2021). Application of biological activity of oxazepine and 2-azetidinone compounds and study of their liquid crystalline behavior. Materials Today: Proceedings, 43, 2040-2050.
33) Aftan, M. M., Talloh, A. A., Dalaf, A. H., & Salih, H. K. (2021). Impact para position on rho value and rate constant and study of liquid crystalline behavior of azo compounds. Materials Today: Proceedings.
34) Aftan, M. M., Toma, M. A., Dalaf, A. H., Abdullah, E. Q., & Salih, H. K. (2021). Synthesis and Characterization of New Azo Dyes Based on Thiazole and Assess the Biological and Laser Efficacy for Them and Study their Dyeing Application. Egyptian Journal of Chemistry, 64(6), 2903-2911.
35) Khalaf, S. D., Ahmed, N. A. A. S., & Dalaf, A. H. (2021). Synthesis, characterization and biological evaluation (antifungal and antibacterial) of new derivatives of indole, benzotriazole and thioacetyl chloride. Materials Today: Proceedings. 47(17), 6201-6210.
36) Dalaf, A. H., Jumaa, F. H., & Salih, H. K. (2021). Preparation, Characterization, Biological Evaluation and Assess Laser Efficacy for New Derivatives of Imidazolidin-4-one. International Research Journal of Multidisciplinary Technovation, 3(4), 41-51.
37) Dalaf, A. H., Jumaa, F. H., & Salih, H. K. (2021). MULTIDISCIPLINARY TECHNOVATION. Red, 15(A2), C44H36N10O8.
38) Dalaf, A. H., Jumaa, F. H., Aftana, M. M., Salih, H. K., & Abd, I. Q. (2022). Synthesis, Characterization, Biological Evaluation, and Assessment Laser Efficacy for New Derivatives of Tetrazole. In Key Engineering Materials (Vol. 911, pp. 33-39). Trans Tech Publications Ltd.
39) Lee, J., Yim, Y., Kim, S., Choi, M. H., Choi, B. S., Lee, Y., & Min, D. H. (2016). In-depth investigation of the interaction between DNA and nano-sized graphene oxide. Carbon, 97, 92-98.